Modeling the large scale physics of

Causal Dynamical Triangulations

Bachelor thesis

By Wouter Houthoff

Supervisors:
Dr. J.H. Cooperman & Prof. Dr. R. Loll

June 24, 2015

Abstract

In this thesis we will be looking at the quantum gravity theory of causal dynamical triangulations (CDT) in its classical limit. We try to find out which theory of gravity describes this limit best: Einstein-Hilbert or Hořava-Lifshitz gravity. In order to do this, the expressions for the spatial volume as a function of time and associated fluctuations are found and compared to data obtained from numerical simulations of causal dynamical triangulations. In order to get these expressions, the field equations with positive cosmological constant of these theories of gravity can be solved for a standard metric of a minisuperspace form to yield the scale factor. The expression for the spatial 2-volume can be calculated out of the scale factor of this metric. Using perturbation theory, an equation governing fluctuations in the 2-volume can be derived. After discretization the obtained spatial 2-volume and the spectrum of fluctuations approximates the classical limit of causal dynamical triangulations rather nicely. In both the Einstein-Hilbert and the Hořava-Lifshitz case, the obtained equations will be fit against CDT data, where simulations have been done for the spatial 2-volume, and associated fluctuations, of evolving universes through time with physical properties. Since the Hořava-Lifshitz action is a generalization of the Einstein-Hilbert action, it is expected that the former gives a better fit to the data. However, this turned out to be true only for specific cases.

Contents

1 Causal dynamical triangulations

For a long time people have been looking for a fully quantised theory of gravity. Causal dynamical triangulations (CDT) is one of the candidates to fulfil that roll. It is a non-perturbative theory that already has promising results in dimensions $d = 2$, $d = 3$ and especially in $d = 4$.[1, 2] It makes use of the path integral approach, which looks like

$$Z = \int Dg\ e^{iS[g]/\hbar}. \tag{1}$$

The integral on the right hand side gives a quantum state Z in the quantum theory of gravity. This expression shows the integral over all paths of the exponent of the action S, dependent on a metric g. For the simulations done in this thesis the Einstein-Hilbert action is used, defined later on. Each path in this path integral represents a universe in the case of quantum gravity. In order to do calculations with this path integral, it needs to be discretized to

$$Z = \sum_T m(T)\ e^{iS(T)/\hbar}, \tag{2}$$

where $m(T)$ is called the measure[1] and T a specific triangulation. The measure is calculated as the inverse of the order of the automorphism group of each triangulation T. Each triangulation represents a different way of building up discrete spacetimes with small building blocks of Minkowski space. With these building blocks, expression 2 can be seen as a summation over all universes. In $2+1$ dimensions[1] these building blocks are tetrahedra, see figure 1.[1, 2, 3, 4, 5, 6] These forms have multiple great benefits, but mostly they are simple to use.

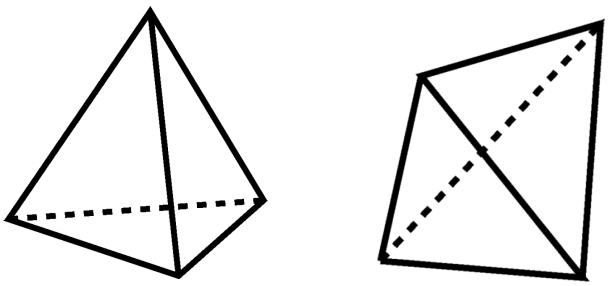

(a) (b)

Figure 1: Two different forms a tetrahedron can have in $2+1$ dimensions. The space coordinates make a surface into the paper, whereas the time coordinate goes upwards.

There are three kinds of tetrahedra in a (2+1)-dimensional set-up. First, there are tetrahedra where three vertices evolve into one vertex over time (figure 1(a) is an example of such a tetrahedron), called (3,1) tetrahedra. Next there are tetrahedra where one vertex evolves into three vertices over time, (1,3) tetrahedra. Due to symmetry reasons, a spacetime build up out of tetrahedra always has the same number of (3,1) as (1,3) tetrahedra. Lastly, there are (2,2) tetrahedra, where a tetrahedron with two vertices evolves into a tetrahedron with two different vertices, see figure 1(b).
These tetrahedra can describe different universes when glued together in various ways. The

[1] Meaning 2 space and 1 time dimensions.

tetrahedra are always glued face-to-face so that they form layers for each discrete point in time, also called a time slice. In 2+1 dimensions, for each time slice the tetrahedra form a 2-sphere. The number of tetrahedra used per simulation is a direct link to what discrete 3-volume each universe has. The number of time-like (3,1), (1,3) and (2,2) tetrahedra ($N_3^{(3,1)}$, $N_3^{(1,3)}$ and $N_3^{(2,2)}$) stand for the discrete spacetime 3-volume, where the total spacetime volume is the summation of those three values, also called the number of 3-simplices. If one looks at a specific time slice, the number of space-like triangles N_2^{SL} one finds represents the discrete spatial 2-volume, also called the number of spatial 2-simplices.

When restricted to summing over these so-called 'causal' spacetimes, equation 2 carries a well-defined Wick rotation. This is the name for when a manifold with Lorentzian signature is changed to a manifold with Euclidean signature. After Wick rotation expression 2 becomes a partition function,

$$Z = \sum_T m(T)\ e^{-S(T)/\hbar}. \tag{3}$$

The Einstein-Hilbert action used in this expression can be expressed in terms of the number of 0-simplices and the number of 3-simplices used per simulation[7],

$$S^{(EH)}(T) = -k_0 N_0 + k_3 N_3, \tag{4}$$

where k_0 and k_3 and the coupling constants. This Wick rotation is necessary for the numerical simulation done in CDT.[4]

Simulations can be done regarding the calculation of the volume of various universes. These universes are born, the volume evolves in time, and the universes die again. Each particular simulation is run at a fixed number of 3-simplices and a fixed number of time slices. Three examples of universes are given in figure 2, where the vertical axes represent time and the horizontal axes state the spatial 2-volume of each universe in each point in time.[4]

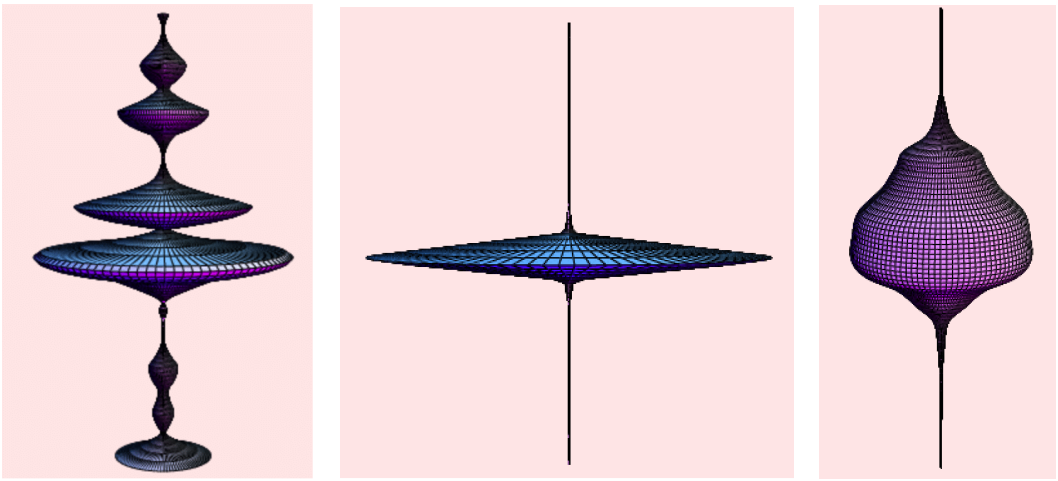

(a) (b) (c)

Figure 2: Three examples of simulations where a universe gets born, evolves and dies. The vertical axes represents time, whereas the horizontal axes states the volume of each universe.

Each of these simulations in figure 2 represents a different phase of quantum geometry. Since the phase represented in figure 2(c) is the only one with universes having physical properties, we will only consider universes of such a phase, which is phase C.
Since CDT is a quantum mechanical theory, it is possible to look at expectation values of observables in the quantum state defined by expression 2 of all universes with phase C. The expectation values of various observables may be classically approximated by Einstein-Hilbert gravity and Hořava-Lifshitz gravity. In this thesis we look at two properties: the spatial 2-volume of classical Einstein-Hilbert and Hořava-Lifshitz gravity and the semi-classical fluctuations in that spatial 2-volume. We approach the spatial 2-volume classically because we are looking at entire universes. In other words, we examine the large scale physics of CDT, making it a classical limit to approach. The fluctuations on that volume are approached semi-classically since those are quantum fluctuations on a classical volume. We compare the values of these properties to the expectation value of the number of 2-simplices and the expectation value of the fluctuations of all universes found in numerical simulations of CDT, and state which of the theories of gravity best describes CDT in its classical limit.

2 Models

As stated before, multiple simulations of growing and dying universes can be done. The typical form of such a data set for a universe in phase C in 2+1 dimensions is shown is figure 3, where the expectation value of the spatial number of 2-simplices at each time slice is set against the discrete number of time slices.

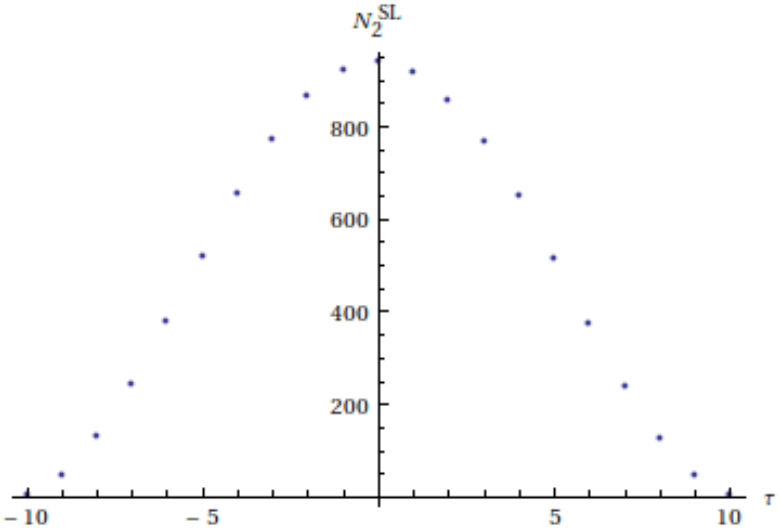

Figure 3: This is a CDT obtained simulation of the expectation value of all universes that are born, grow and die. The horizontal axis represents the discrete number of time slices used in the simulation, while the vertical axis shows the expectation value of the spatial number of 2-simplices at each time slice. In this simulation 21 time slices are used.

Quantum mechanics state that locally there are very small fluctuations in this volume[8]. These fluctuations represent the deviation from the ensemble average,

$$n_2^{SL}(\tau) = N_2^{SL}(\tau) - < N_2^{SL}(\tau) > . \tag{5}$$

In this thesis we look at the correlation between n_2^{SL} at two different times, $< n_2^{SL}(\tau)\ n_2^{SL}(\tau') >$, because the expectation value of $n_2^{SL}(\tau)$ is zero, with

$$< n_2^{SL}(\tau)\ n_2^{SL}(\tau') >= \frac{1}{K-1} \sum_{j=1}^{K} \left[N_{2j}^{SL}(\tau) - < N_2^{SL}(\tau) > \right] \left[N_{2j}^{SL}(\tau') - < N_2^{SL}(\tau') > \right] \tag{6}$$

and

$$< n_2^{SL}(\tau) >= \frac{1}{K} \sum_{j=1}^{K} N_{2j}^{SL}(\tau). \tag{7}$$

Since $< n_2^{SL}(\tau)\ n_2^{SL}(\tau') >$ is a $T \times T$-matrix with indices τ and τ', we can diagonalise it to get its eigenvectors and eigenvalues. An example of such a dataset can be seen in figures 4 and 5.

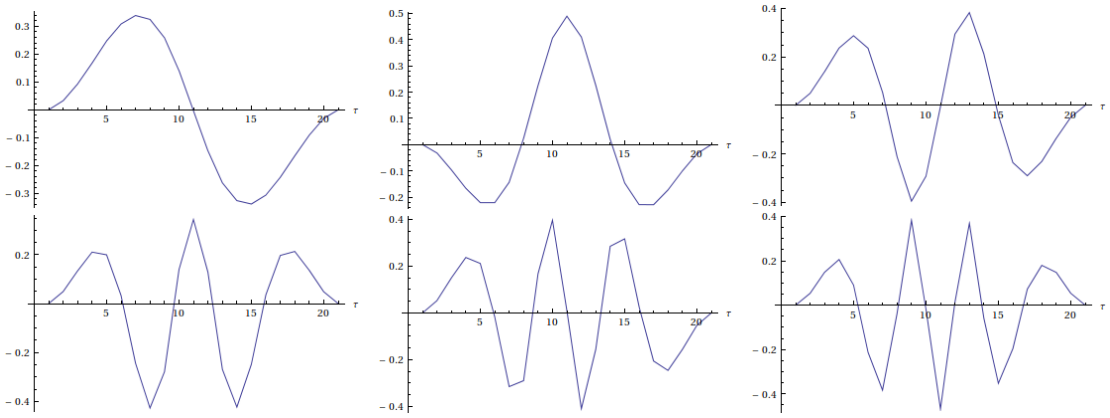

Figure 4: The first six eigenvectors of the fluctuations in the 2-volume of the same simulation that used 21 time slices.

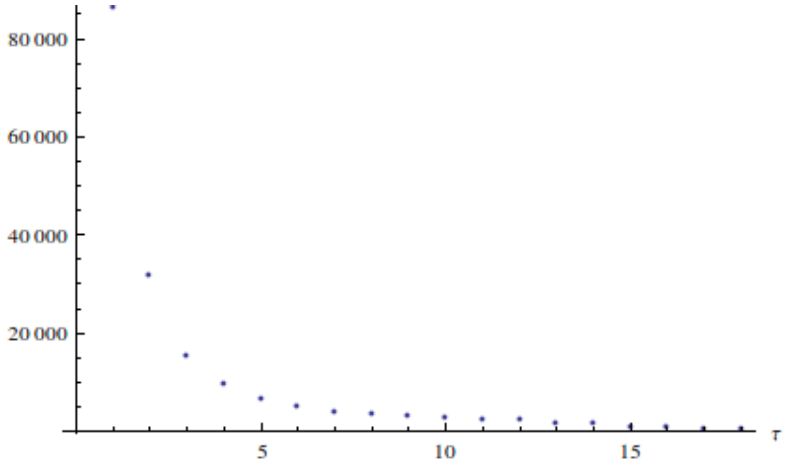

Figure 5: The eigenvalues of the fluctuations in the 2-volume of the same simulation that used 21 time slices.

In order to describe the number of 2-simplices and its fluctuations, two models have been created that possibly fit the data. In the first model use has been made of the Einstein-Hilbert action, which will be shown and explained later on in section 2.1. In the second model the Einstein-Hilbert action has been generalized to the so-called Hořava-Lifshitz action, section 2.2. Since the Hořava-Lifshitz action is a generalization of the Einstein-Hilbert action, it has two extra parameters which can be adjusted later on to get the best fits possible. Note that the Hořava-Lifshitz model might not give better fits in a statistically significant way. Both models use a classical approach to fit the expectation value of the spatial 2-simplices, and a semi-classical approach to model the spectrum of fluctuations. The expression for the spatial 2-volume, V_0, is obtained by solving the equations of motion from the action. In order to get the expression for the fluctuations in the volume, perturbation theory has been applied on the action around the classical solution,

$$V(t) \rightarrow V_0(t) + \delta V(t) \tag{8}$$
$$S \rightarrow S_0 + S_1 + S_2 + \ldots, \tag{9}$$

where V_0 is the solution to the equation of motion found for the 2-volume. S_0 is simply the action with V_0 filled in. In both cases the first order perturbation S_1 will become zero. This happens because the expression of the 2-volume satisfies the equation of motion. The equation of motion is obtained by partial integration,

$$\begin{aligned} S_1[V_0, \dot{V}_0] &= \int dt \ \frac{\delta S[V,\dot{V}]}{\delta \ V(t)}\bigg|_{V_0,\dot{V}_0} \delta \ V(t) + \int dt \ \frac{\delta S[V,\dot{V}]}{\delta \ \dot{V}(t)}\bigg|_{V_0,\dot{V}_0} \delta \ \dot{V}(t) \\ &= \int dt \left(\frac{\delta S}{\delta \ V(t)} - \frac{\partial}{\partial t} \frac{\delta S}{\delta \ \dot{V}(t)} \right) \delta \ V(t) = 0. \end{aligned} \tag{10}$$

The second order perturbation however, S_2, will be the first non-trivial, non-zero term;

$$\begin{aligned} S_2[V_0, \dot{V}_0, \ddot{V}_0] &= \frac{1}{2} \iint dt \ dt' \ \frac{\delta^2 S[V,\dot{V}]}{\delta V(t) \ \delta V(t')}\bigg|_{V_0,\dot{V}_0} \delta V(t) \ \delta V(t') \\ &+ \frac{1}{2} \iint dt \ dt' \ \frac{\delta^2 S[V,\dot{V}]}{\delta V(t) \ \delta \dot{V}(t')}\bigg|_{V_0,\dot{V}_0} \delta V(t) \ \delta \dot{V}(t') \\ &+ \frac{1}{2} \iint dt \ dt' \ \frac{\delta^2 S[V,\dot{V}]}{\delta \dot{V}(t) \ \delta V(t')}\bigg|_{V_0,\dot{V}_0} \delta \dot{V}(t) \ \delta V(t') \\ &+ \frac{1}{2} \iint dt \ dt' \ \frac{\delta^2 S[V,\dot{V}]}{\delta \dot{V}(t) \ \delta \dot{V}(t')}\bigg|_{V_0,\dot{V}_0} \delta \dot{V}(t) \ \delta \dot{V}(t') \end{aligned} \tag{11}$$

In both models we start off with the general, diagonal, three-dimensional metric

$$g_{\alpha\beta} = \begin{pmatrix} \sigma g_{tt} & 0 & 0 \\ 0 & a^2(t) & 0 \\ 0 & 0 & a^2(t)\sin^2(\theta) \end{pmatrix}. \tag{12}$$

Here σ is plus or minus one, depending on respectively Euclidean or Lorentzian signature, g_{tt} is the time-time component of this metric, which is a positive constant, and $a^2(t)$ is called the scale factor, depending on time. This rather general metric is the so-called minisuperspace approximation for the action used later on in equation 13. The goal is to find an expression for the two-dimensional volume of this 'universe' depending on time. This volume can be calculated out of the scale factor, which intuitively can be seen as a radius in the minisuperspace model. This specific minisuperspace is a 2-sphere at each time, and has been chosen because we only measure the volume as a function of time from CDT simulations, ignoring all of the other geometrical information. This scale factor has been found for the Einstein-Hilbert action in section 2.1 and the Hořava-Lifshitz action in section 2.2.

2.1 Einstein-Hilbert gravity

The Einstin-Hilbert action is our starting point,

$$S_{(2+1)-EH} = \frac{1}{16\pi G}\int dt\ d^2x\ N\sqrt{g}\ \{R - 2\Lambda\}\,. \tag{13}$$

Of course, Λ is the cosmological constant. N is called the lapse rate, which is the square root of g_{tt}. g represents the determinant of the spatial metric, so $\sqrt{g} = a^2(t)\sin\theta$. The factor R is the Ricci scalar of the three dimensional metric. The Ricci scalar represents the curvature in each point in spacetime[9], and is given by

$$R = g^{\mu\nu}R_{\mu\nu}, \tag{14}$$

where the Ricci tensor is

$$R_{\mu\nu} = R^{\sigma}_{\mu\sigma\nu} = \partial_\sigma\Gamma^\sigma_{\mu\nu} - \partial_\nu\Gamma^\sigma_{\mu\sigma} + \Gamma^\sigma_{\delta\sigma}\Gamma^\delta_{\mu\nu} - \Gamma^\sigma_{\delta\nu}\Gamma^\delta_{\mu\sigma}. \tag{15}$$

Γ is called the Christoffel symbol and is given by

$$\Gamma^\gamma_{\alpha\beta} = \frac{1}{2}g^{\gamma\delta}\left(\partial_\alpha g_{\beta\delta} + \partial_\beta g_{\delta\alpha} - \partial_\delta g_{\alpha\beta}\right). \tag{16}$$

This Christoffel symbol has nine non-zero terms for the metric of equation 12, namely

$$\begin{aligned}
\Gamma^0_{11} &= -\frac{a\dot{a}}{\sigma g_{tt}} & \Gamma^1_{22} &= -\sin\theta\cos\theta \\
\Gamma^0_{22} &= -\frac{a\dot{a}}{\sigma g_{tt}}\sin^2\theta & \Gamma^2_{20} &= \Gamma^2_{02} = \frac{\dot{a}}{a} \\
\Gamma^1_{10} &= \Gamma^1_{01} = \frac{\dot{a}}{a} & \Gamma^2_{12} &= \Gamma^2_{21} = -\frac{\cos\theta}{\sin\theta}.
\end{aligned} \tag{17}$$

Now, the Ricci scalar can be calculated in terms of the scale factor:

$$R = \frac{2}{a^2} - \frac{2\dot{a}^2}{\sigma g_{tt}a^2} - \frac{4\ddot{a}}{\sigma g_{tt}a}. \tag{18}$$

After the lapse rate, the square root of g and the Ricci scalar are filled into the Einstein-Hilbert action, one can integrate over the two-volume to get an extra factor of 4π due to the sine, making the action look like

$$S_{(2+1)-EH} = \frac{\sqrt{g_{tt}}}{2G}\int dt\left(1 + \frac{\dot{a}^2}{\sigma g_{tt}} - \Lambda a^2\right). \tag{19}$$

The action is an integral over the Lagrangian, which gives the equation of motion. With

$$S = \int L dt \tag{20}$$

and the equation of motion

$$\frac{d}{dt}\left(\frac{\partial L}{\partial\dot{a}}\right) = \frac{\partial L}{\partial a}, \tag{21}$$

one can find the following differential equation:

$$\ddot{a} + \sigma g_{tt} \Lambda a = 0. \tag{22}$$

A solution to this equation is given by[6, 10, 11, 12]

$$a(t) = l_{ds} \cos\left(\frac{\sqrt{\sigma g_{tt}}\, t}{l_{ds}}\right), \tag{23}$$

where l_{ds} is the de Sitter length, with $l_{ds} = 1/\sqrt{\Lambda}$. The spatial 2-volume of the de Sitter spacetime can be calculated out of the scale factor. As seen before, the scale factor is analogous to a radius. This means that the 2-volume can be found by integrating the scale factor over the entire volume of a time slice,

$$V_2(t) = \int d\theta d\phi\ \sqrt{g}\ =\ \int d\theta d\phi\ sin(\theta)\ a^2(t)\ =\ 4\pi a^2(t). \tag{24}$$

If this expression is filled in for the scale factor, one gets

$$V_2(t) = 4\pi l_{ds}^2 \cos^2\left(\frac{\sqrt{\sigma g_{tt}}\, t}{l_{ds}}\right). \tag{25}$$

This classical expression represents the birth and death of the de Sitter universe. When the metric holds an Euclidian signature (meaning $\sigma = +1$), the timelength in which this universe lives is only physically meaningful for $t \in [-\pi l_{ds}/2\sqrt{g_{tt}}; \pi l_{ds}/2\sqrt{g_{tt}}]$. With the Lorentzian signature ($\sigma = -1$), the ranges are much broader, namely $t \in [-\infty; \infty]$.
In the CDT simulation, fluctuations in the 2-volume have been observed. This is why we look for them in our classical theories. These quantum fluctuations can be made visible in the semi-classical approach, where a slight perturbation is applied to the spatial 2-volume[14, 15]. So, equation 19 can be rewritten in terms of the 2-volume according to equation 24, so

$$S_{(2+1)-EH}[V, \dot{V}] = \frac{\sqrt{g_{tt}}}{32\pi G} \int dt \left(16\pi + \frac{\dot{V}^2}{\sigma g_{tt} V} - 4\Lambda V\right). \tag{26}$$

Now one can apply the perturbation according to equation 11, which gives

$$S_2[V_0, \dot{V_0}, \ddot{V_0}] = \frac{\sigma}{32\pi G l_{ds}} \int d\tilde{t}\ \delta V \frac{1}{V_0} \left(-\frac{l_{ds}^2}{g_{tt}} \frac{\dot{V_0}^2}{V_0^2} + \frac{l_{ds}^2}{g_{tt}} \frac{\ddot{V_0}}{V_0} + \frac{l_{ds}}{\sqrt{g_{tt}}} \frac{\dot{V_0}}{V_0} \frac{\partial}{\partial \tilde{t}} - \frac{\partial^2}{\partial \tilde{t}^2}\right) \delta V \tag{27}$$

with $\tilde{t} = \sqrt{g_{tt}}\ t/l_{ds}$. In this action the 2-volume can be filled in, ending with the expression

$$S_2^{(2+1)-EH} = \begin{cases} -\frac{1}{128\pi^2 G l_{ds}^3} \int d\tilde{t}\ \delta V \sec^2\tilde{t} \left(2\sec^2\tilde{t} + 2\tan\tilde{t}\frac{\partial}{\partial\tilde{t}} + \frac{\partial^2}{\partial\tilde{t}^2}\right)\delta V & \sigma = +1 \\ \frac{1}{128\pi^2 G l_{ds}^3} \int d\tilde{t}\ \delta V \mathrm{sech}^2\tilde{t} \left(-2\mathrm{sech}^2\tilde{t} - 2\tanh\tilde{t}\frac{\partial}{\partial\tilde{t}} + \frac{\partial^2}{\partial\tilde{t}^2}\right)\delta V & \sigma = -1 \end{cases} \tag{28}$$

In section 3 this expression is rewritten into a discrete form and used to numerically fit the CDT obtained data.

2.2 Hořava-Lifshitz gravity

In the Hořava-Lifshitz model the same steps are taken as in the Einstein-Hilbert model in order to obtain a better fit to the data. The only real difference is the ansatz, where not the Einstein-Hilbert action, but the Hořava-Lifshitz action is used[11, 12, 13],

$$S_{(2+1)-HL} = \frac{1}{16\pi G}\int dt\ d^2x\ N\sqrt{g}\ \left\{\sigma(\lambda K_2^2 - K_{ij}K^{ij}) - 2\Lambda + bR_2 - \gamma R_2^2\right\}. \tag{29}$$

We use the same metric in this action as before in equation 12, so that the lapse rate and the square root of g are the same. Furthermore, one can spot the three different parameters λ, b and γ, which can be fine-tuned later on to get the best fit possible. However, for $\lambda, b = 1$ and $\gamma = 0$, the Hořava-Lifshitz action reduces to the Einstein-Hilbert action, meaning that it is a generalisation of the Einstein-Hilbert case. The Ricci scalar R_2 in this case is the Ricci scalar over the spatial coordinates only. K_{ij} is called the extrinsic curvature, which states how much a spatial slice is curved within the whole spacetime. K_2 is the trace of the spatial tensor K_{ij}, meaning $K_2 = g^{ij}K_{ij}$. K_{ij} is defined by

$$K_{ij} = e_i^\alpha e_j^\beta \nabla_\alpha n_\beta, \tag{30}$$

with $e_i^\alpha = \partial x^\alpha/\partial x^i$ and $\nabla_\alpha n_\beta = \partial_\alpha n_\beta - \Gamma^\gamma_{\alpha\beta} n_\gamma$.[9] The Christoffel symbol is already calculated in equation 17. The vector n_β is the normal vector on each time slice. This means that n_β itself is a timelike vector. Since it also is a unit normal vector,

$$\sqrt{n_\beta n^\beta} = \sqrt{g_{\alpha\beta}n^\alpha n^\beta} = -1 \ \longrightarrow\ n_\beta = (\sqrt{g_{tt}}, 0, 0). \tag{31}$$

Now the extrinsic curvature can be calculated in terms of the scale factor;

$$K_{ij}K^{ij} = \frac{2}{g_{tt}}\frac{\dot{a}^2}{a^2} \tag{32}$$

$$K^2 = \frac{4}{g_{tt}}\frac{\dot{a}^2}{a^2} \tag{33}$$

The Ricci scalar is calculated analogously to equation 14, only now for the spatial metric,

$$R_2 = g^{ij}R^{(2)}_{ij} = \frac{2}{a^2}. \tag{34}$$

After filling in the expressions in equations 32, 33 and 34 into the action in equation 29 and integrating over all spatial coordinates, one is left with

$$\begin{aligned} S_{(2+1)-HL} &= \frac{\sqrt{g_{tt}}}{2G}\int dt\left\{\frac{\sigma(2\lambda-1)}{g_{tt}}\dot{a}^2 - \Lambda a^2 + b - \frac{2\gamma}{a^2}\right\} \\ &= \frac{1}{2\kappa^2}\int dt\left\{\dot{a}^2 - \omega^2 a^2 + b' - \frac{\xi}{a^2}\right\}, \end{aligned} \tag{35}$$

where

$$\begin{aligned}\omega^2 &= \sigma\frac{g_{tt}\Lambda}{2\lambda-1}\\ \xi &= \sigma\frac{2g_{tt}\gamma}{2\lambda-1}\\ b' &= \sigma\frac{g_{tt}b}{2\lambda-1}\\ \kappa^2 &= \sigma\frac{\sqrt{g_{tt}}G}{2\lambda-1}.\end{aligned} \tag{36}$$

Now the equations of motion can be determined again, see equations 20 and 21, for equation 35 to get the following differential equation:

$$\ddot{a} + \omega^2 a - \frac{\xi}{a^3} = 0. \tag{37}$$

The solution to this equation is

$$a(t) = \frac{1}{\omega A}\sqrt{(\omega^2 A^4 - \xi)\cos^2(\omega t + \psi) + \xi}. \tag{38}$$

Here A and ψ stand for integration constants.[11] When the limit of Einstein-Hilbert gravity is taken[2] A needs to be set to the de Sitter length l_{ds}. ψ is just a choice of the origin for the time coordinate, which is set to zero. If done so, the scale factor in the Einstein-Hilbert case of equation 23 emerges.
Now equation 24 is used to rewrite the scale factor in terms of the spatial 2-volume, so

$$V_2(t) = \frac{4\pi}{\omega^2 A^2}\left\{\left(\omega^2 A^4 - \xi\right)\cos^2(\omega t + \psi) + \xi\right\}. \tag{39}$$

Again, according to equation 24, the action in equation 35 can be rewritten in terms of the spatial 2-volume to get

$$S_{(2+1)-HL} = \frac{1}{2\kappa^2}\int dt\left\{\frac{1}{16\pi}\frac{\dot{V}^2}{V} - \frac{\omega^2}{4\pi}V + b' - 4\pi\xi\frac{1}{V}\right\}. \tag{40}$$

Now a perturbation is added where, again, the first order will be zero because this expression is also proportional to the equation of motion. The second order perturbation can be calculated according to equation 11, so

$$S_2[V_0, \dot{V}_0, \ddot{V}_0] = \frac{1}{32\pi\omega\kappa^2}\int d\tilde{t}\ \delta V\frac{1}{V_0^2}\left(-\frac{\dot{V_0}^2}{V_0} + \ddot{V}_0 - 64\pi^2\xi\frac{1}{V_0} + \omega\dot{V}_0\frac{\partial}{\partial\tilde{t}} - \omega^2 V_0\frac{\partial^2}{\partial\tilde{t}^2}\right)\delta V. \tag{41}$$

Since the 2-volume is now a known expression, it can be filled in to equation 41 to get

$$\begin{aligned}S_2^{(2+1)-HL} = &-\frac{\omega^3 A^2}{64\pi^2\kappa^2}\int d\tilde{t}\ \delta V\ \frac{1}{\left(\Omega\cos^2\tilde{t} + \xi\right)^3}\Bigg[\left(\omega^4 A^8 - \xi^2\right)\cos^2\tilde{t}\\ &+\left(\omega^2 A^4 + \xi\right)\xi + \Omega\cos\tilde{t}\sin\tilde{t}\left(\Omega\cos^2\tilde{t} + \xi\right)\frac{\partial}{\partial\tilde{t}}\\ &+\left(\frac{1}{2}\Omega^2\cos^4\tilde{t} + \xi\Omega\cos^2\tilde{t} + \frac{1}{2}\xi^2\right)\frac{\partial^2}{\partial\tilde{t}^2}\Bigg]\delta V.\end{aligned} \tag{42}$$

[2]Meaning, if $\lambda, b = 1$ and $\gamma = 0$.

In this last expression $\Omega = \omega^2 A^4 - \xi$ and $\tilde{t} = \sqrt{\sigma g_{tt}}\ t/\sqrt{2\lambda - 1}\ l_{ds}$. A simple check can be performed to see if equation 42 has the right Einstein-Hilbert limit in equation 28, again with $\lambda, b = 1$ and $\gamma = 0$ filled in.

2.3 Discretisation of the models

Since the CDT simulations are done for a discrete path integral, the formulas from equations 25, 28, 39 and 42 need to be rewritten in a discrete form. Since the Einstein-Hilbert case is a simplification of the Hořava-Lifshitz case, only the calculation of the discrete analogue of the spatial 2-volume and the integrand of the second order perturbation of the action in the Hořava-Lifshitz case are needed. Then, the limit of $\lambda = b = 1$ and $\gamma = 0$ can be taken again to obtain the Einstein-Hilbert variant.

2.3.1 The number of spatial 2-simplices

In equation 39 the Hořava-Lifshitz spatial 2-volume

$$V_2(t) = \frac{4\pi}{\omega^2 A^2}\left\{\left(\omega^2 A^4 - \xi\right)\cos^2(\omega t + \psi) + \xi\right\}$$

was found. A discrete analogue to this continuous expression, called the number of spatial 2-simplices, has been derived out of this equation. The data obtained from simulations are organized in such a way that $\psi = 0$. Now equation 39 can be rewritten as

$$\begin{aligned} V_2(t) &= 4\pi A^2\left\{\left(1 - \frac{2\gamma}{A^4\Lambda}\right)\cos^2\left(\frac{\sqrt{g_{tt}}\ t}{\tilde{l}}\right) + \frac{2\gamma}{A^4\Lambda}\right\} \\ &= 4\pi A^2\left\{(1-a)\cos^2\left(\frac{\sqrt{g_{tt}}\ t}{\tilde{l}}\right) + a\right\}, \end{aligned} \tag{43}$$

with $\omega^2 = g_{tt}/l_{ds}^2(2\lambda - 1) = g_{tt}/\tilde{l}^2$ and $a = 2\gamma/A^4\Lambda$. Note that the condition $\sigma = +1$ has been taken into account here, so that we are looking at de Sitter space with Euclidean signature. We now constrain the spacetime volume to the value V_3, because the simulations are done at fixed number of 3-simplices. The total spacetime 3-volume can be given by integrating the spatial 2-volume over time

$$\begin{aligned} V_3 &= \sqrt{g_{tt}}\int_{-\frac{\tau}{2}}^{\frac{\tau}{2}} dt\ V_2(t) \\ &= 4\pi\sqrt{g_{tt}}\left(\frac{\pi(\xi + A^4\omega^2)}{2A^2\omega^3} + \frac{\xi}{A^2\omega^2}\left(\tau - \frac{\pi}{\omega}\right)\right) \\ &= 4\pi A^2\left(\frac{\pi\tilde{l}}{2}(a+1) + a(\sqrt{g_{tt}}\ \tau - \pi\tilde{l})\right), \end{aligned} \tag{44}$$

where τ is the finite time extent of the continuous time coordinate and a our newly defined parameter.[6] Now the expressions for the spatial 2-volume (43) and the spacetime 3-volume (44) are combined to

$$V_2 = \frac{V_3}{\tilde{l}}\frac{1}{a\left(\frac{\sqrt{g_{tt}}\ \tau}{\tilde{l}} - \pi\right) + \frac{\pi}{2}(1+a)}\left\{(1-a)\cos^2\left(\frac{\sqrt{g_{tt}}\ t}{\tilde{l}}\right) + a\right\}. \tag{45}$$

The total volume V_3 can be linked to the discrete total volume of all of the tetrahedra used in each simulation in units of the lattice spacing, according to

$$V_3 = C_3\tilde{a}^3 N_3. \tag{46}$$

In this condition $\tilde{a}$ stands for the lattice spacing of the tetrahedra used to build this triangulation, and C_3 is the discrete spacetime 3-volume of such tetrahedra.[6] In general, the continuum time coordinate t scales with $V_3^{-1/3}$. Analogously we expect the discrete time coordinate τ to scale with $N_3^{-1/3}$, making the expression

$$dt = \left(\frac{V_3}{N_3}\right)^{1/3} \Delta\tau, \tag{47}$$

where $\Delta\tau$, the discrete time steps, is taken to be 1. As seen before in (44), the total volume V_3 is the integral over the spatial 2-volume V_2 with respect to time. Similarly, the total number of spacetime 3-simplices N_3 can be seen as the summation over all time slices of the total number spatial 2-simplices N_2. This means that equation 47 gives

$$\sqrt{g_{tt}}\ V_2(t) V_3^{\frac{1}{3}}(t) = 2\ (1+\xi)\ C_3\ \tilde{a}^3 N_3^{\frac{1}{3}}(\tau) N_2^{SL}(\tau). \tag{48}$$

Here ξ stands for the proportion

$$\xi = \frac{N_3^{(2,2)}}{N_3^{(1,3)} + N_3^{(3,1)}}. \tag{49}$$

Now we can plug equations 46 and 47 back in to equation 48 to make

$$N_2^{SL} = \frac{\sqrt{g_{tt}}}{2\ (1+\xi)} \frac{N_3}{V_3} \frac{V_3^{\frac{1}{3}}}{N_3^{\frac{1}{3}}} V_2. \tag{50}$$

Here V_2 can be filled in from equation 45 to get the discrete number of spatial 2-simplices in the Hořava-Lifshitz case,

$$N_2^{HL} = \frac{N_3^{(3,1)}}{s_0 \left(N_3^{(3,1)}\right)^{1/3}} \frac{1}{\frac{aT}{s_0\left(N_3^{(3,1)}\right)^{1/3}} + \frac{\pi}{2}(1-a)} \left\{ (1-a)\cos^2\left(\frac{\tau}{s_0\left(N_3^{(3,1)}\right)^{1/3}}\right) + a \right\}, \tag{51}$$

with the parameter

$$\frac{1}{s_0} = \frac{\sqrt{g_{tt}}\ V_3^{\frac{1}{3}}}{\tilde{l} 2^{\frac{1}{3}} (1+\xi)^{\frac{1}{3}}}. \tag{52}$$

Now we can take the Einstein-Hilbert limit with $\lambda = b = 1$ and $\gamma = 0$, in this case meaning $a = 0$, to get

$$N_2^{EH} = \frac{2}{\pi} \frac{N_3^{(3,1)}}{s_0 \left(N_3^{(3,1)}\right)^{1/3}} \cos^2\left(\frac{\tau}{s_0\left(N_3^{(3,1)}\right)^{1/3}}\right). \tag{53}$$

The expressions 51 and 53 are compared to data from CDT simulations. As stated before, each dataset is made with different values for 3-simplices N_3 and number of time slices T. This means that for each dataset the two free parameters s_0 and a can be chosen to give the best fit in the Hořava-Lifshitz case. All other parameters have disappeared from the calculation. In the Einstein-Hilbert case only the parameter s_0 remains.

2.3.2 The integrand of the second order perturbation

Equation 42 states the expression for the action of Hořava-Lifshitz gravity perturbed to second order. There is an constant in front of equation 42 for which we can determine its numerical value by fitting the model to $< n_2^{SL}(\tau)\ n_2^{SL}(\tau') >$ from equation 6, but for our purposes we do not care about the value of this constant. Taking this last remark into consideration, the integrand of equation 42 with the perturbation δV removed from both sides looks like

$$\begin{aligned} - \quad & \frac{1}{\left((1-a)\cos^2\tilde{t}+a\right)^3}\Bigg[\left(1-a^2\right)\cos^2\tilde{t}+a+a^2 \\ + \quad & (1-a)\cos\tilde{t}\sin\tilde{t}\left((1-a)\cos^2\tilde{t}+a\right)\frac{\partial}{\partial\tilde{t}} \\ + \quad & \left(\frac{1}{2}(1-a)^2\cos^4\tilde{t}+a(1-a)\cos^2\tilde{t}+\frac{1}{2}a^2\right)\frac{\partial^2}{\partial\tilde{t}^2}\Bigg], \end{aligned} \tag{54}$$

where $\tilde{t} = \sqrt{g_{tt}}\ t/\sqrt{2\lambda-1}\ l_{ds}$ and the free parameter $a = 2\gamma l^2/A^4$. Again note that this integrand has been taken for the Euclidean signature, so $\sigma = +1$. This expression can be seen as a differential operator in front of the perturbation δV. What we use to model the data of $< n_2^{SL}(\tau)\ n_2^{SL}(\tau') >$ with, is $< \delta V(t)\ \delta V(t') >$. This expectation value is per definition the integral

$$< \delta V(t)\ \delta V(t') > = \frac{1}{Z}\int D\delta V\ \delta V(t)\delta V(t')e^{iS[\delta V]}, \tag{55}$$

where the action $S[\delta V]$ is the action as defined in equation 28 for the Einstein-Hilbert case, and equation 42 for the Hořava-Lifshitz case. The state Z is

$$Z = \int D\delta V\ e^{iS[\delta V]}, \tag{56}$$

so that the expectation value normalises. The outcome for the integral of this expectation value is proporional to the inverse of the differential operator seen in equation 54. Now we can apply the same condition as in equation 47 to get the discretisation of equation 54:

$$\begin{aligned} - \quad & \frac{2(1+a)}{\left((1-a)\cos^2\tilde{\tau}+a\right)^2} - 2s_0\left(N_3^{(3,1)}\right)^{1/3}(1-a)\cos\tilde{\tau}\sin\tilde{\tau}\left((1-a)\cos^2\tilde{\tau}+a\right)^{-2}\frac{\Delta}{\Delta\tau} \\ - \quad & s_0^2\left(N_3^{(3,1)}\right)^{2/3}\left((1-a)\cos^2\tilde{\tau}+a\right)^{-1}\frac{\Delta^2}{\Delta\tau^2} \end{aligned} \tag{57}$$

where $\tilde{\tau} = \tau/s_0\left(N_3^{(3,1)}\right)^{1/3}$ and $\Delta/\Delta\tau$ a discrete derivative. In the Einstein-Hilbert limit, $a = 0$, it looks like

$$-2\sec^4\tilde{\tau} - 2s_0\left(N_3^{(3,1)}\right)^{1/3}\tan\tilde{\tau}\ \sec^2\tilde{\tau}\frac{\Delta}{\Delta\tau} - s_0^2\left(N_3^{(3,1)}\right)^{2/3}\sec^2\tilde{\tau}\frac{\Delta^2}{\Delta\tau^2}. \tag{58}$$

These last two equations, 57 and 58 can be seen as a differential operator in between of the fluctuations δV. These operators have eigenvectors and corresponding eigenvalues. The eigenvectors and -values are used to derive the spectrum of fluctuations.

3 Data analysis

Now that the plotting formulas have been calculated, the fits can be made. For this section, the program Mathematica has been used. In every simulation the data points have been fit according to the parameter s_0 in the Einstein-Hilbert case, and parameters s_0 and a in Hořava-Lifshitz gravity. In order to see how good of a fit each simulation is, the 'chi-squared' value per degree of freedom has been calculated. The closer this number is to zero, the better the fit. These χ^2_{pdf} values have been calculated for three cases: the spatial 2-volume, the fluctuations and for a so called 'combined' fit. For the spatial 2-volume the optimal values of s_0 and a correspond to the lowest χ^2_{pdf} value. Its value is calculated according to

$$\chi^2_{vol} = \sum_{t=2}^{T-1} \frac{(\text{data} - \text{fit})^2}{(\text{error in data})^2}, \tag{59}$$

$$\chi^2_{pdf\ vol} = \frac{\chi^2}{T - \#\text{fitparameters}}, \tag{60}$$

with T the number of data points being fit. For $t = 1, T$ the data sets have specific fixed values, which means that de error is zero. Because of this reason, those data points have been held out of the calculation of the χ^2_{pdf} values. Also note that the higher the number of variables used in each fitting function, the higher the χ^2_{pdf} value gets. This means that the Hořava-Lifshitz case, which has one extra parameter, does not always has to give statistically better fits.
In the fit for the fluctuations the same values of s_0 and a have been taken as for the fit to the spatial 2-volume. In order to calculate its χ^2_{pdf} value, the right fitting model needs to be made. This is the so-called inverse covariance matrix (ICM), and is build up out of the eigenvectors (V_t) and eigenvalues (λ_t) of the operators in equations 57 and 58,

$$\text{ICM} = \sum_{t=1}^{T} \frac{1}{\lambda_t} V_t V_t^T, \tag{61}$$

where V_t^T is the transponent of eigenvector number t. The χ^2_{pdf} value is now calculated according to

$$\chi^2_{fluc} = \sum_{t=2}^{T-1} \sum_{\tau=2}^{t} \frac{(\text{data} - \rho\ \text{ICM})^2}{(\text{error in data})^2}, \tag{62}$$

$$\chi^2_{pdf\ fluc} = \frac{\chi^2}{T - \#\text{fitparameters}}, \tag{63}$$

Note that only half of the fit values of the matrices are being taken into consideration. This is so because the matrices are mirror symmetric. Also note the extra free parameter ρ. In section 2.3.2 it was explained that the constant factor in from of equation 42 has been left out of the expression. The reason for this is that the free parameter ρ can be chosen to give the best fit possible anyway, making the a priory unknown constant redundant.
In the combined fit the parameter values have been chosen to give a lowest possible value for the summation of $\chi^2_{pdf\ vol}$ and the $\chi^2_{pdf\ fluc}$, so

$$\chi^2_{pdf,total} = \chi^2_{pdf,vol}[s, a] + \chi^2_{pdf,fluc}[s, a, \rho]. \tag{64}$$

Out of various datasets two distinguished cases have been analysed, the case where the number of time slices per simulation increases while the number of 3-simplices used have been kept constant, and the case where the number of 3-simplices increases while the number of time slices have been kept constant.

3.1 Changing the number of time slices at fixed number of 3-simplices

In this section fits have been made to datasets with the number of time slices $T = 13, 17, 21, 25$ at the number of 3-simplices used $N_3 = 30850$. This means that four cases have been simulated. In each simulation approximately 10^5 universes were generated and averaged for the spatial 2-volume and corresponding fluctuations. All cases have the same amount of space-time 3-volume. All simulations have been done at bare coupling constant $k_0 = 1$ (see equation 4).

3.1.1 Fit of the spatial 2-volume

For these fits of the number of spatial 2-simplices against a discrete number of time slices, with the Einstein-Hilbert 2-volume as classical limit, equation 53 has been used.

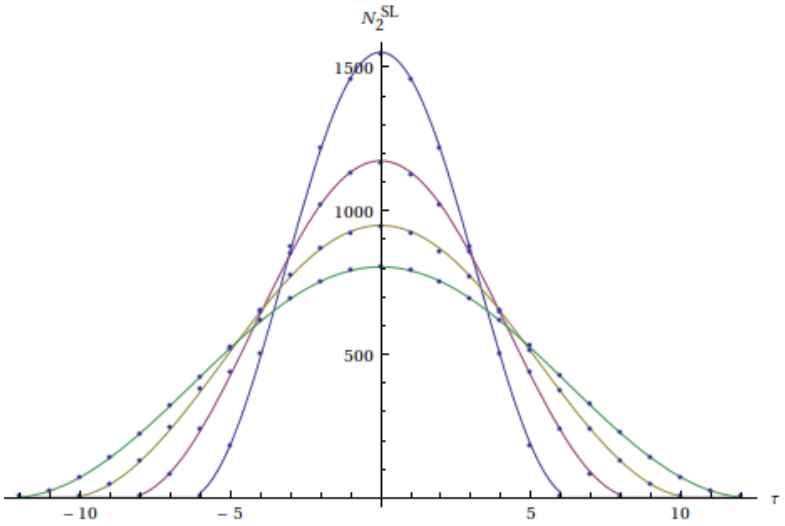

Figure 6: The blue line is the fit done for $T = 13$ time slices, the red line has $T = 17$, the yellow fit uses $T = 21$ time slices and the green fit has $T = 25$ time slices. The horizontal axes state the number of time slices, while the vertical axes represents the number of spacial 2-simplices on that time slice. The area under the curve represents the number of spacetime 3-simplices used, which is constant in all four cases.

For the next graphs equation 51 of the volume in the Hořava-Lifshitz case has been used. The datapoints fit are the same as in figure 6.

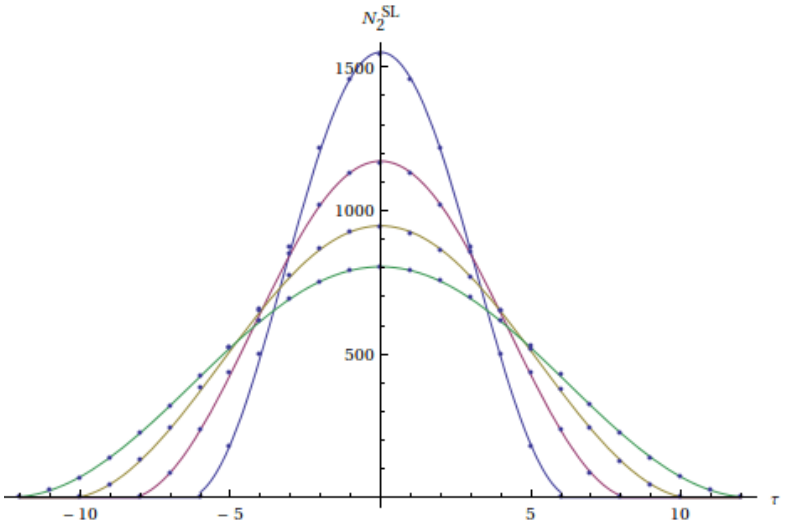

Figure 7: These fits contain the same datapoints as in figure 6, only here the Hořava-Lifshitz case from equation 51 has been used. Again $T = 13, 17, 21, 25$ respectively.

To see which fits are better, the χ^2_{pdf} values have been calculated and stated in table 1.

T	$s_{0\ EH}$	$\chi^2_{pdf\ EH}$	$s_{0\ HL}$	a_{HL}	$\chi^2_{pdf\ HL}$
13	0.190416	98.1280	0.198168	-0.041616	3.01075
17	0.251378	64.9558	0.259040	-0.026975	2.19027
21	0.310805	38.7624	0.317400	-0.016409	7.48319
25	0.366519	7.73903	0.366203	0.000545	7.67937

Table 1: This is the table concerning the graphs in figures 6 and 7. Seen here is the number of time slices used, the best fit parameter values s_0 and a in the Einstein-Hilbert and the Hořava-Lifshitz cases and the χ^2_{pdf} values of all fits.

A plot has been made of these χ^2_{pdf} values in table 1 against the number of time slices, see figure 8.

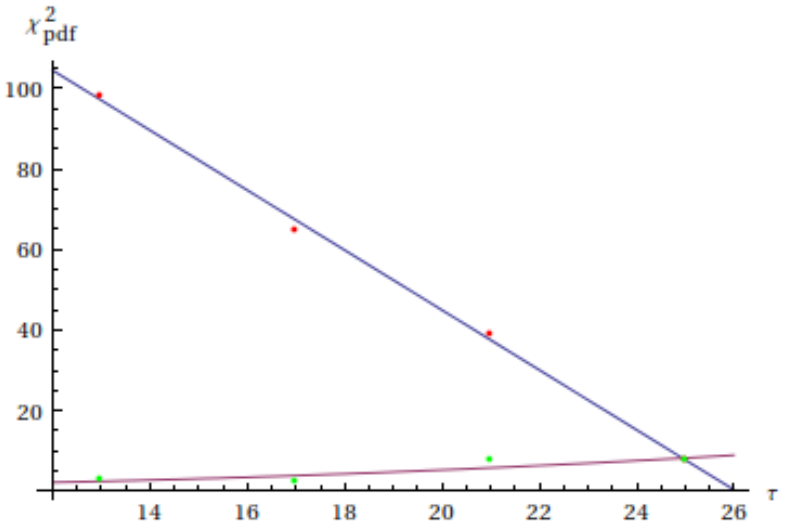

Figure 8: A plot of the χ^2_{pdf} values of the 2-volume against the number of time slices. The blue line represents the Einstein-Hilbert case, while the red line shows the Hořava-Lifshitz case.

It is seen that for the 2-volume, the Hořava-Lifshitz case in general clearly has better fits to the CDT data than the Einstein-Hilbert case for $T < 25$. For $T = 25$ time slices however, the difference in the χ^2_{pdf} value is too small to make the same conclusion.

3.1.2 Fit of the fluctuations

To fit the eigenvectors of the fluctuations, the eigenvectors of equation 58 for the Einstein-Hilbert case and equation 57 for the Hořava-Lifshitz case have been calculated. In the next few graphs the red eigenvectors are the CDT-obtained datapoints, and the blue eigenvectors are the calculated Einstein-Hilbert and Hořava-Lifshitz vectors. Only the first six eigenvectors of each simulation have been shown.

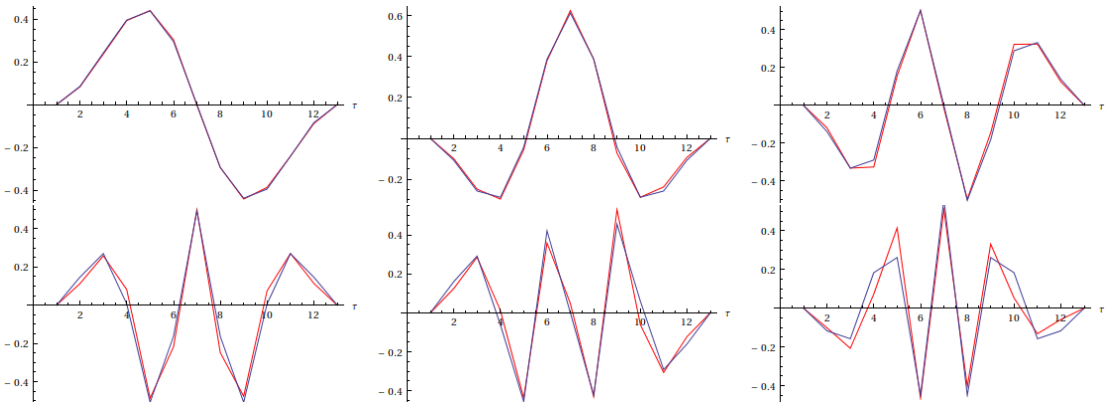

Figure 9: The first six eigenvectors of $T = 13$ in the Einstein-Hilbert case for the data and fit.

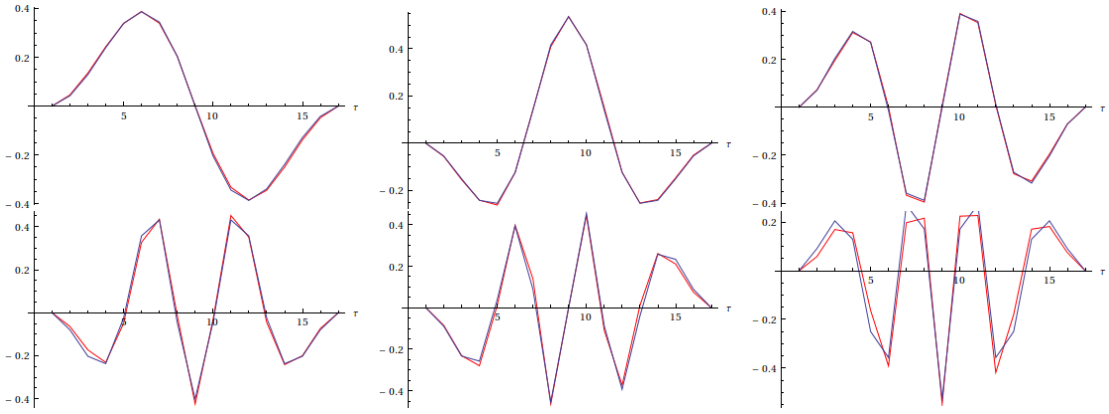

Figure 10: The first six eigenvectors of $T = 17$ in the Einstein-Hilbert case for the data and fit.

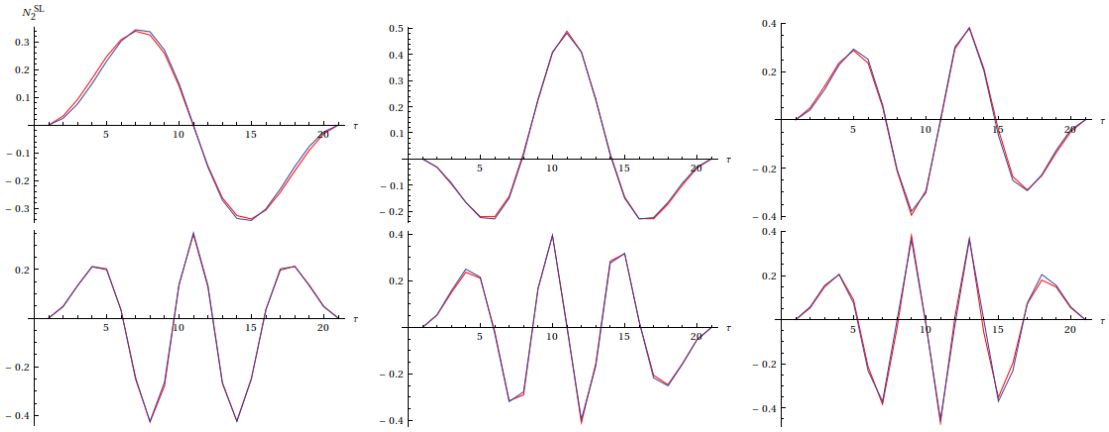

Figure 11: The first six eigenvectors of $T = 21$ in the Einstein-Hilbert case for the data and fit.

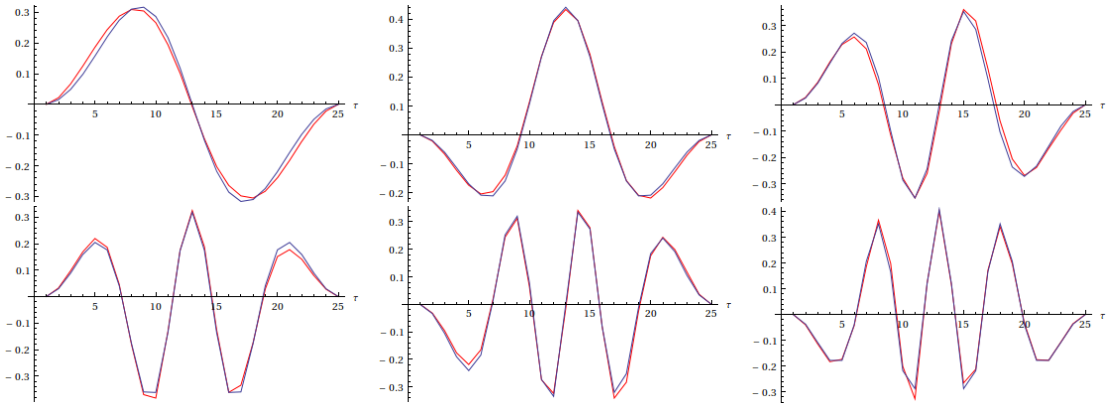

Figure 12: The first six eigenvectors of $T = 25$ in the Einstein-Hilbert case for the data and fit.

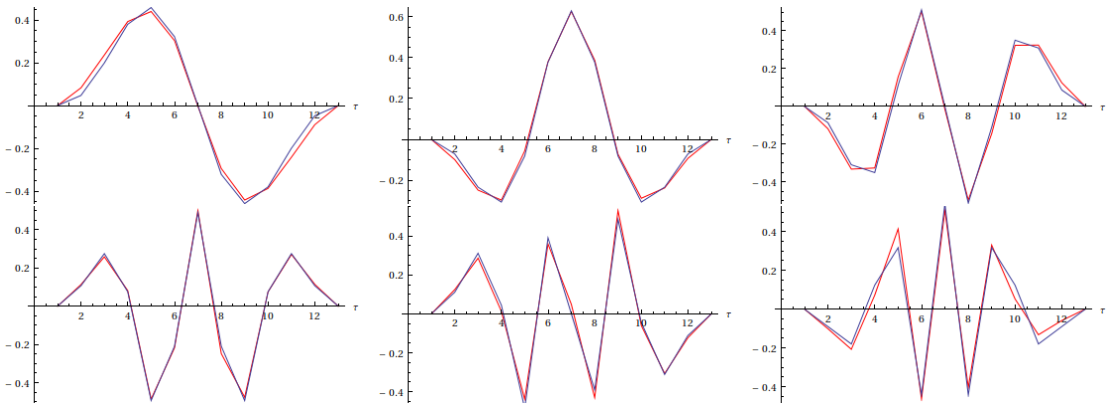

Figure 13: The first six eigenvectors of $T = 13$ in the Einstein-Hilbert case for the data and fit.

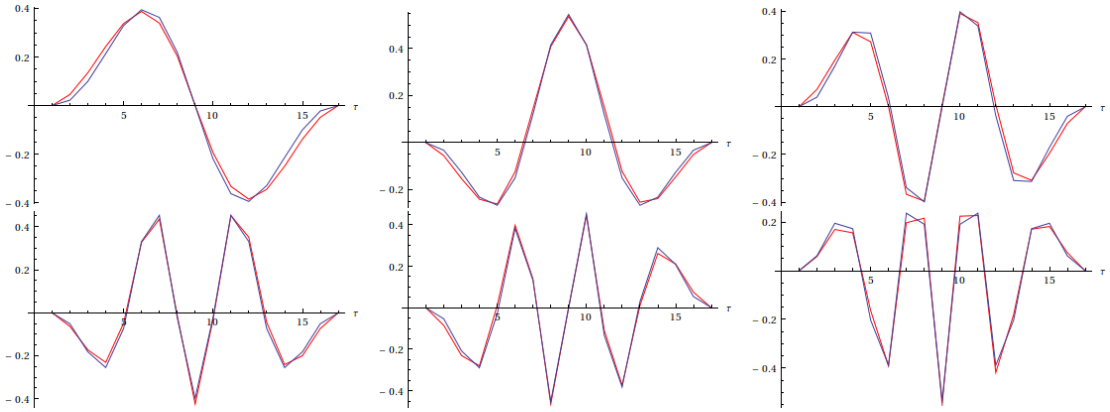

Figure 14: The first six eigenvectors of $T = 17$ in the Einstein-Hilbert case for the data and fit.

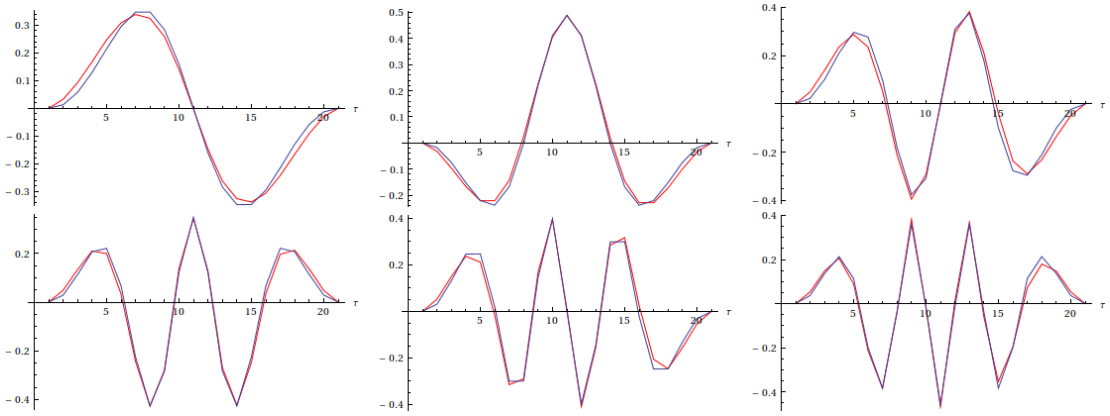

Figure 15: The first six eigenvectors of $T = 21$ in the Einstein-Hilbert case for the data and fit.

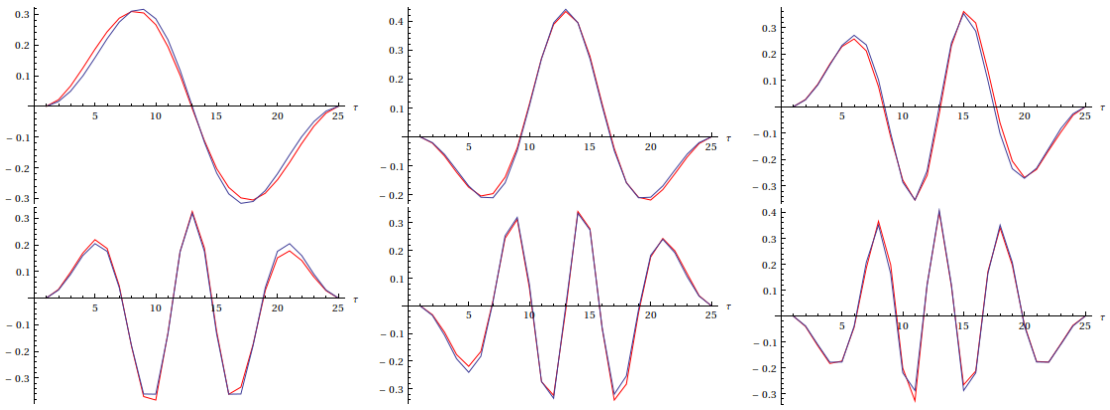

Figure 16: The first six eigenvectors of $T = 25$ in the Einstein-Hilbert case for the data and fit.

The parameter values are taken to be the same as in table 1. Those, and χ^2_{pdf} values, are given in table 2. The χ^2_{pdf} values here are calculated with respect to all the available eigenvectors for that number of time slices[3], and not just the first six.

T	$s_{0\ EH}$	$\chi^2_{pdf\ EH}$	$s_{0\ HL}$	a_{HL}	$\chi^2_{pdf\ HL}$
13	0.190416	15.1191	0.198168	-0.041616	419.615
17	0.251378	38.327	0.259040	-0.026975	579.281
21	0.310805	193.079	0.317400	-0.016409	990.735
25	0.366519	626.571	0.366203	0.000545	576.719

Table 2: This is the table concerning the graphs in figures 9 until 16. Seen here is the number of time slices used, the parameter values s_0 and a in the Einstein-Hilbert and the Hořava-Lifshitz case and the χ^2_{pdf} values of all fits.

The results in table 2 have also been plotted in figure 17.

[3]For $T = 13$ time slices for example, there were 13 eigenvectors. In every simulation however, three eigenvectors did not fit the boundary conditions that they started and ended in zero, and that the total spacetime volume was zero as well. These eigenvectors have been taken out of the calculation of χ^2_{pdf}. So for $T = 13$, only 10 eigenvectors were taken into consideration. For $T = 17$, there were 14, for $T = 21$ there were 18 and for $T = 25$ there were 22.

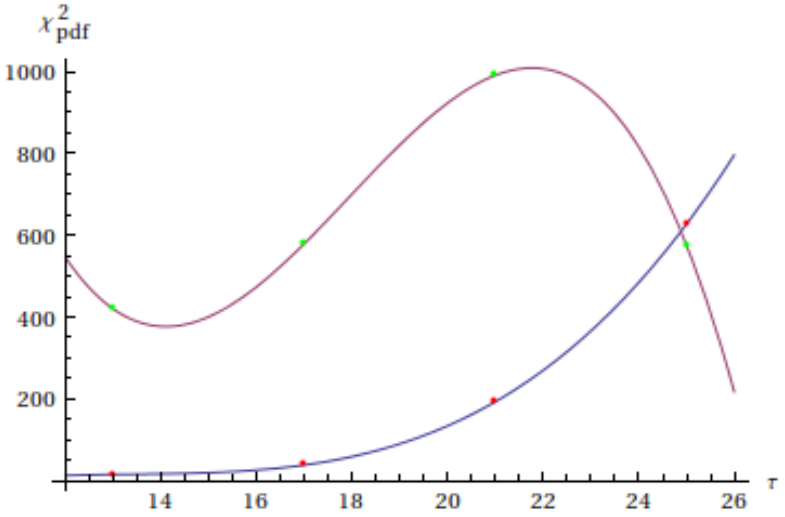

Figure 17: A plot of the χ^2_{pdf} values against the number of time slices of the fluctuations. Again, the blue line represents the Einstein-Hilbert case, and the red line shows the Hořava-Lifshitz case.

In the 2-volume an obviously lower χ^2_{pdf} value in the Hořava-Lifshitz case has been found. The same can not be said for the fluctuations. Here the Hořava-Lifshitz case is way higher than the Einstein-Hilbert case for $T < 25$. For $T = 25$ it is seen that the Hořava-Lifshitz case is indeed a bit smaller, as we would have expected. The reason the Hořava-Lifshitz χ^2_{pdf} value is so much higher is due to the parameter values of s_0 and a for which the fit has been done, since these were taken to be the same as in the spatial 2-volume case. Small changes is those parameter values could create large differences in the χ^2_{pdf} values. To see if this statement is true, the combined fit has been done.

3.1.3 Combined fit

In the combined fit the parameter values of s_0 and a were chosen in such a way that the summation of the χ^2_{pdf} values of the 2-volume and the fluctuations are the lowest. In table 3 the found $\chi^2_{pdf,total}$ values are shown.

T	$s_{0\ EH}$	$\chi^2_{pdf\ EH}$	$s_{0\ HL}$	a_{HL}	$\chi^2_{pdf\ HL}$
13	0.190407	105.066	0.194456	-0.021327	51.4802
17	0.251428	99.1745	0.255640	-0.015035	70.7158
21	0.311241	228.171	0.314792	-0.009801	167.531
25	0.360912	393.709	0.362293	0.005244	217.476

Table 3: The parameter values and χ^2_{pdf} values against the number of time slices used per simulation.

Also for these χ^2_{pdf} values a plot has been made, seen in figure 18.

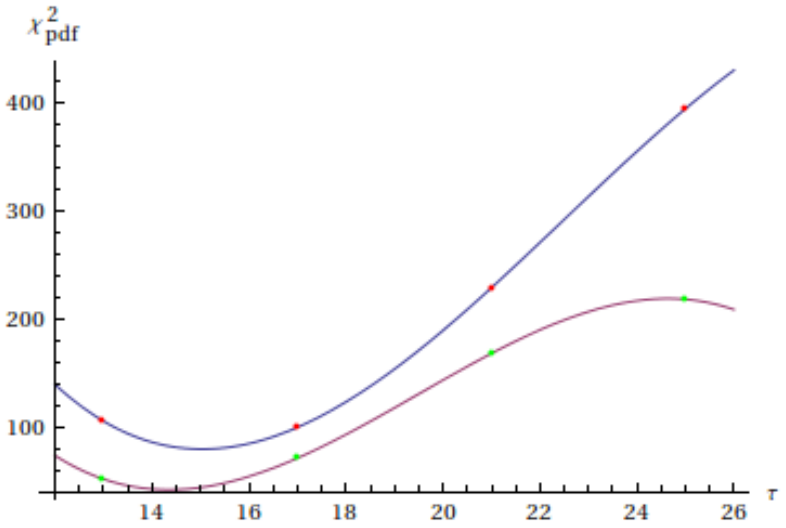

Figure 18: The combined χ^2_{pdf} values plotted against the number of time slices. Again, the blue line represents the Einstein-Hilbert case, and the red line shows the Hořava-Lifshitz case.

This graph shows a lower χ^2_{pdf} value in the Hořava-Lifshitz case in every point. This means that, in general, Hořava-Lifshitz gravity gives better fits to CDT obtained data of the spatial 2-volume and the fluctuations in that volume for a rising number of time slices. It also means that the optimal parameter values for s_0 and a in the spatial 2-volume are not the optimal parameter values for the fluctuations. A plot has been made for the parameter value a in the Hořava-Lifshitz case against the number of time slices, see figure 19

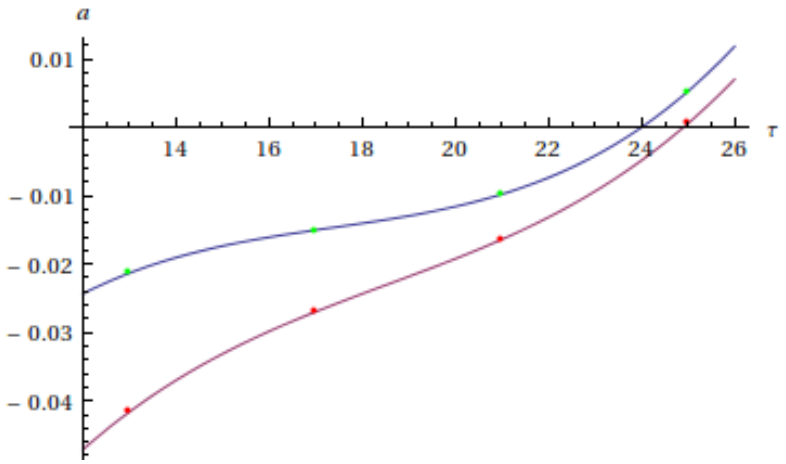

Figure 19: A plot of the parameter value a in the Hořava-Lifshitz case against the number of time slices. The red line represents the values of a for the fit of the 2-volume, while the blue line states the values of a for the combined fits.

It is seen in figure 19 that the parameter value indeed changes significantly for the different fits.

3.2 Changing the number of 3-simplices at fixed number of time slices

In this section fits have been made to datasets with a constant number of time slices $T = 25$ at different numbers of 3-simplices used $N_3 = 30851;\ 65587;\ 102452$. This means that three cases have been simulated. All have the same amount of time before they die, but the space-time 3-volume increases per simulation. This implies that the growth in the space-time 3-volume is found in the spatial 2-volume per time slice alone. Again, all simulations have been done at bare coupling constant $k_0 = 1$.

3.2.1 Fit of the spatial 2-volume

Again, equation 53 has been used in order to make the fit to the number of spatial 2-simplices in the Einstein-Hilbert case, see figure 20.

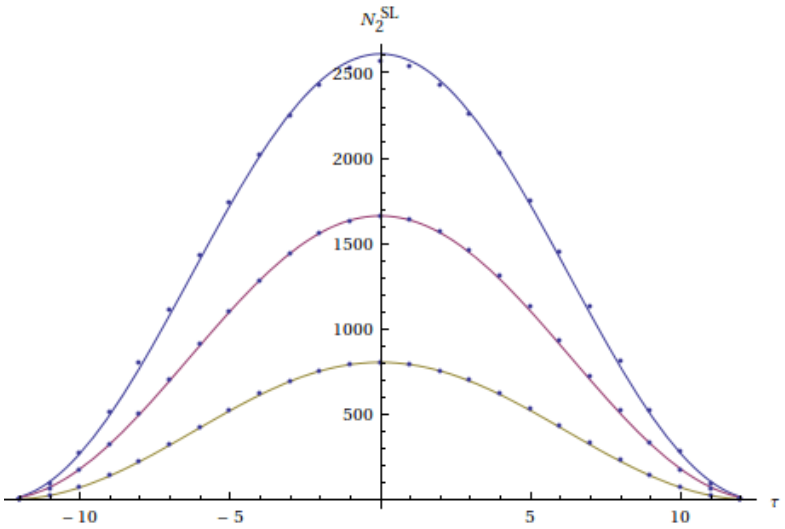

Figure 20: In this figure all three plots represent a universe being born and dying off with $T = 25$ time slices in the Einstein-Hilbert case. The blue fit has a number of 3-simplices used of $N_3 = 30851$, the red fit uses $N_3 = 65587$ and the yellow fit is made for $N_3 = 102452$.

The fits to the data points in figure 20 have also been done in the Hořava-Lifshitz case. Here, equation 51 has been used in order to obtain the graphs in figure 21.

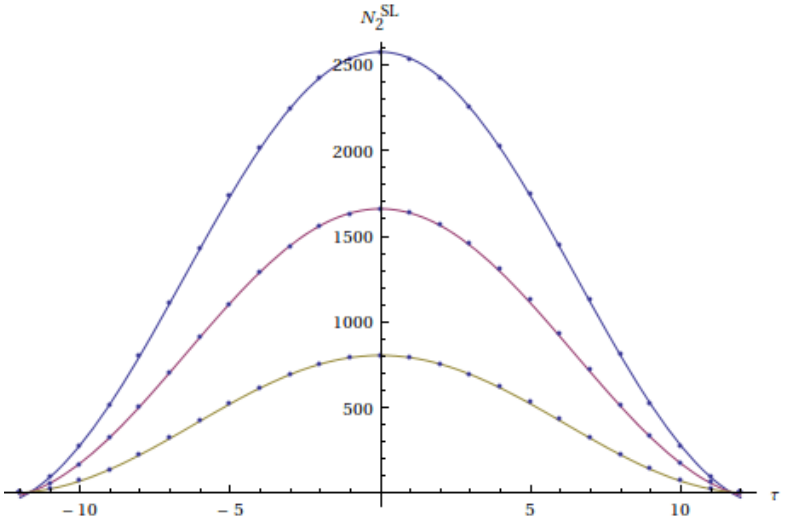

Figure 21: In this figure the universes are fit for the Hořava-Lifshitz case. Again, $T = 25$, and the blue fit has a number of 3-simplices used of $N_3 = 30851$, the red fit uses $N_3 = 65587$ and the yellow fit is made for $N_3 = 102452$.

For these six graphs the χ^2_{pdf} values are listed in table 4.

N_3	$s_{0\ EH}$	$\chi^2_{pdf\ EH}$	$s_{0\ HL}$	a_{HL}	$\chi^2_{pdf\ HL}$
30851	0.366519	7.73903	0.366203	0.000544	7.67937
65587	0.290071	147.504	0.298586	-0.021390	32.6985
102452	0.250851	310.889	0.260465	-0.028605	19.1124

Table 4: This table states the parameter values of s_0 and a, and the χ^2_{pdf} values for the spatial 2-volume in the Einstein-Hilbert and Hořava-Lifshitz cases for increasing 3-simplices.

These χ^2_{pdf} values have been plotted as a function of 3-simplices in figure 22.

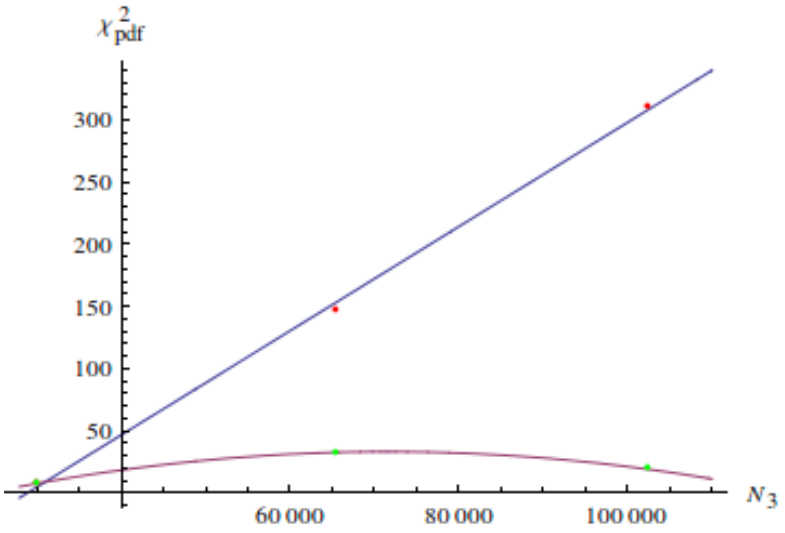

Figure 22: Seen here is the χ^2_{pdf} value of the spatial 2-volume against an increasing number of 3-simplices used per simulation.

Whereas the difference in χ^2_{pdf} of the volume between the Einstein-Hilbert and Hořava-Lifshitz cases grows smaller for an increasing number of time slices (figure 8), it only increases for an increasing number of 3-simplices. The χ^2_{pdf} value for the spatial 2-volume grows linear for the Einstein-Hilbert case, yet in the Hořava-Lifshitz case it stays roughly constant.

3.2.2 Fit of the fluctuations

In order to fit the eigenvectors of the fluctuations, again equations 58 for the Einstein-Hilbert case and 57 for the Hořava-Lifshitz case have been taken into consideration. As before, the parameter values of s_0 and a have been taken to be the same as in the fit to the volume. In figures 23 through 28 the red eigenvectors show the CDT obtained data points, and the blue eigenvectors are from the Einstein-Hilbert and Hořava-Lifshitz cases.

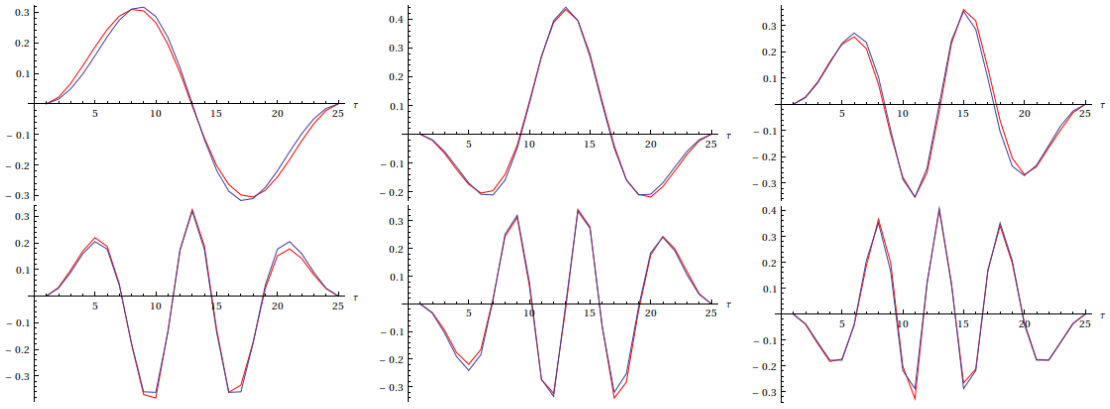

Figure 23: The first six eigenvectors of $N_3 = 30851$ in the Einstein-Hilbert case for data and fit.

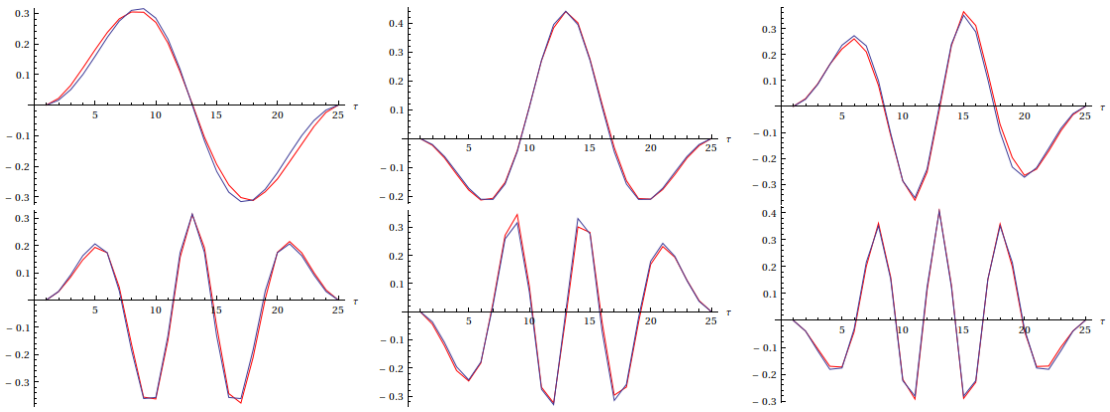

Figure 24: The first six eigenvectors of $N_3 = 65587$ in the Einstein-Hilbert case for data and fit.

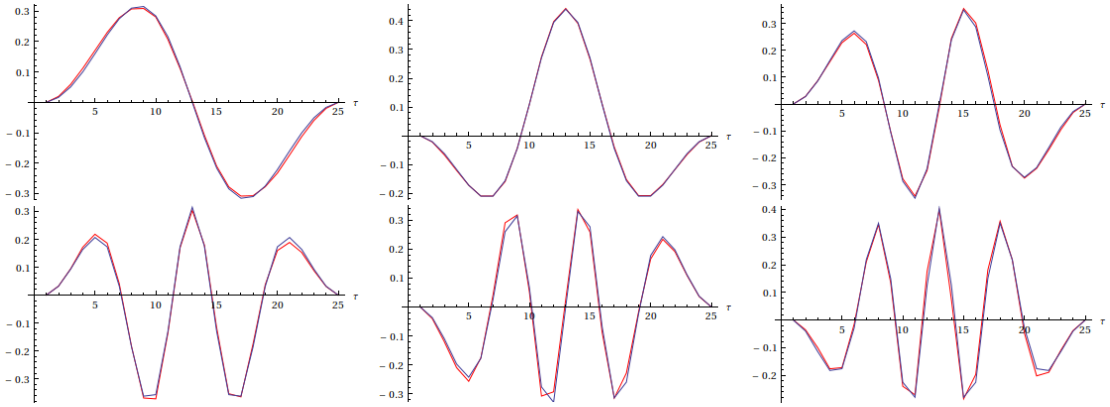

Figure 25: The first six eigenvectors of $N_3 = 102452$ in the Einstein-Hilbert case for data and fit.

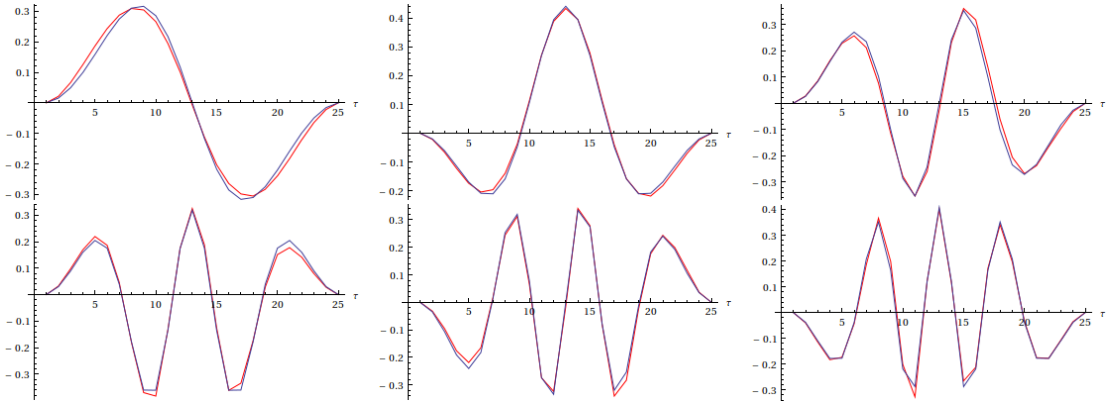

Figure 26: The first six eigenvectors of $N_3 = 30851$ in the Hořava-Lifshitz case for data and fit.

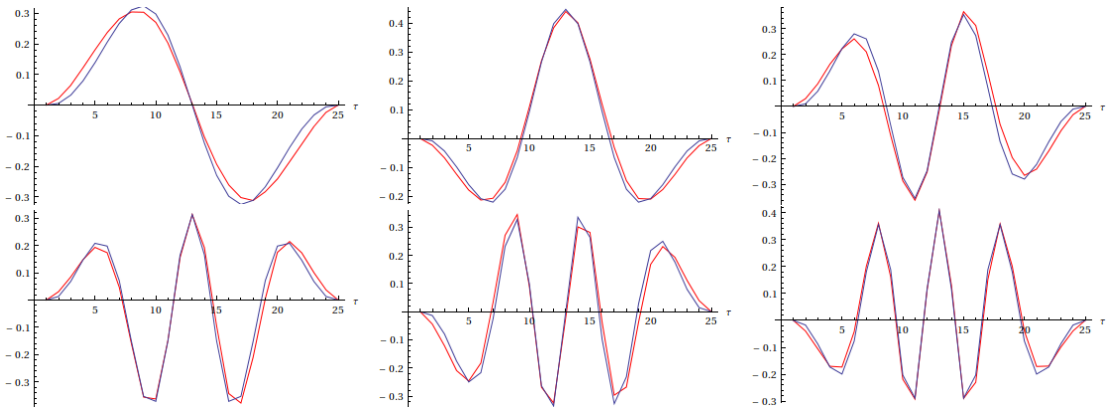

Figure 27: The first six eigenvectors of $N_3 = 65587$ in the Hořava-Lifshitz case for data and fit.

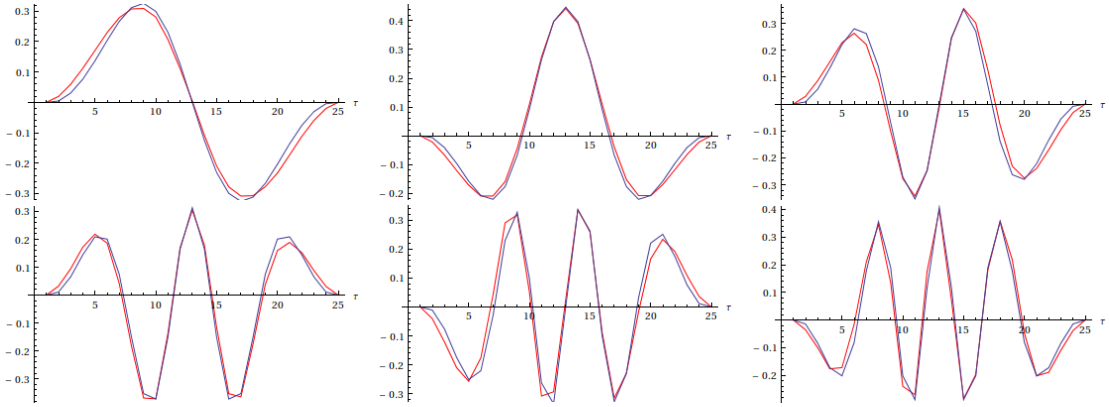

Figure 28: The first six eigenvectors of $N_3 = 102452$ in the Hořava-Lifshitz case for data and fit.

All three simulations[4] have 25 eigenvectors, since the number of time slices used is $T = 25$. Again, three eigenvectors were considered non-physical and were taken out of the calculation. For the remaining 22 eigenvectors the χ^2_{pdf} values per simulation are listed in table 5.

N_3	$s_{0\ EH}$	$\chi^2_{pdf\ EH}$	$s_{0\ HL}$	a_{HL}	$\chi^2_{pdf\ HL}$
30851	0.366519	626.571	0.366203	0.000544	576.719
65587	0.290071	451.612	0.298586	-0.021390	2077.18
102452	0.250851	115.807	0.260465	-0.028605	1523.60

Table 5: This table states the parameter values of s_0 and a, and the χ^2_{pdf} values in the Einstein-Hilbert and Hořava-Lifshitz cases for increasing 3-simplices for the eigenvectors of the fluctuations.

In figure 29 the resulting χ^2_{pdf} values are plotted as a function of the number of 3-simplices.

[4] $N_3 = 30851;\ 65587;\ 102452$

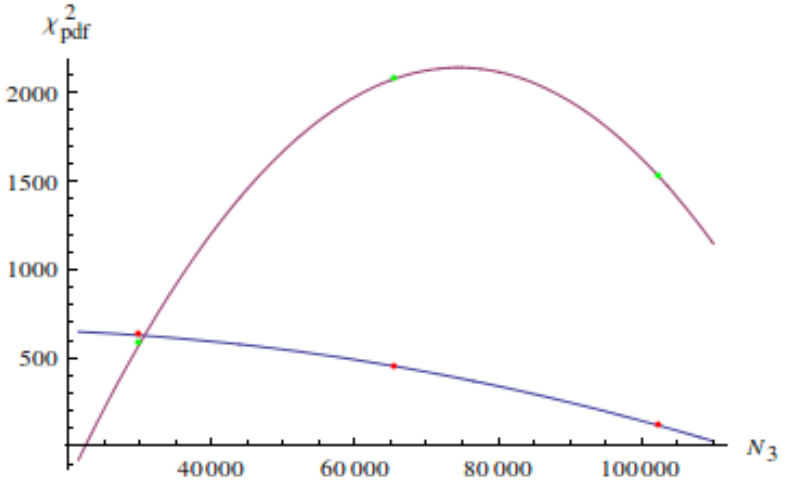

Figure 29: A plot of the χ^2_{pdf} values against the number of 3-simplices for the eigenvectors of the fluctuations. The blue line represents the Einstein-Hilbert case and the red line shows the Hořava-Lifshitz case.

Noticeable is the peak in the χ^2_{pdf} values of the Hořava-Lifshitz curve of $\chi^2_{pdf\ HL} = 2077.18$. This value is too high to state anything meaningful. In section 3.2.3 another fit is done where the parameter values of s_0 and a have been chosen to be optimal for the summation of the χ^2_{pdf} values of the 2-volume and the fluctuations, instead of just for the 2-volume alone.

3.2.3 Combined fit

In table 6 the outcome of the optimal parameter values in the combined fit, along with the χ^2_{pdf} values have been listed.

N_3	$s_{0\ EH}$	$\chi^2_{pdf\ EH}$	$s_{0\ HL}$	a_{HL}	$\chi^2_{pdf\ HL}$
30851	0.360912	393.709	0.362293	0.005244	217.476
65587	0.290592	587.964	0.286606	0.007310	380.334
102452	0.250978	413.097	0.254721	-0.011189	267.479

Table 6: This table represents the parameter values optimal in the combined fit and the accompanied χ^2_{pdf} values.

These outcomes have been plotted in figure 30 a function of the number of 3-simplices.

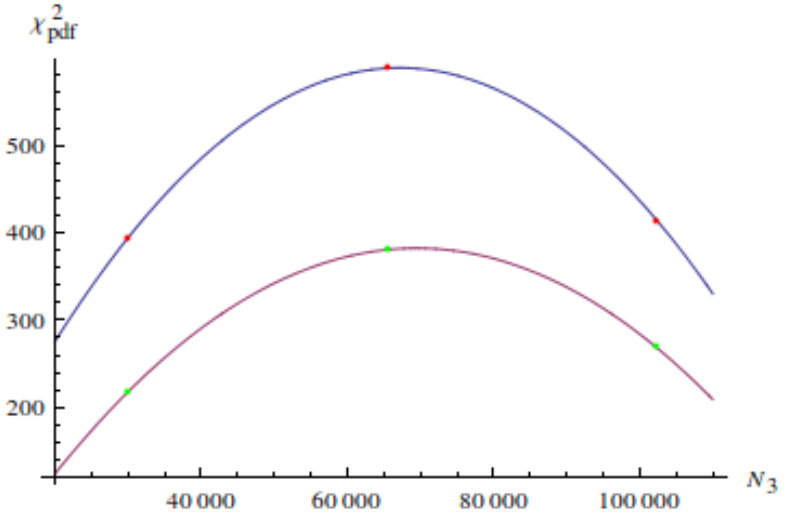

Figure 30: The plot of the combined χ^2_{pdf} values against the number of 3-simplices used. The blue line represents the Einstein-Hilbert case and the red line shows the Hořava-Lifshitz case.

Visible is that the Hořava-Lifshitz case has an overall better fit to the data than the Einstein-Hilbert case, which is in agreement with the findings of section 3.1.3. Again, the optimal values of the free parameter a for the fit of the spatial 2-volume and for the combined fit in the Hořava-Lifshitz case are seen below in figure 31.

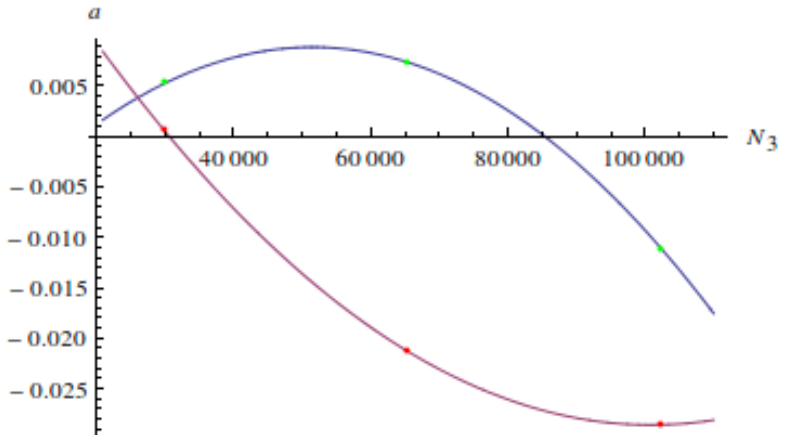

Figure 31: A plot of the parameter value a in the Hořava-Lifshitz case against the number of 3-simplices used per simulation. The red line represents the values of a for the fit of the 2-volume, while the blue line states the values of a for the combined fits.

In general the parameter values for a for the fit of the spatial 2-volume lie lower than the values for the combined fit.

4 Conclusions

The models created in sections 2.1 and 2.2 are both shown to be able to fit the simulations done in CDT. Initially, it was expected that Hořava-Lifshitz gravity would have a better fit to the data than Einstein-Hilbert gravity, since it is a generalisation of the latter one. This is seen in the fact that the Hořava-Lifshitz case had three extra free parameters to begin with, namely λ, b and γ, as seen in equation 29. These parameters could be chosen in such a way the Einstein-Hilbert case would show up again. However, two of these parameters fell out of the equation, leaving only the extra parameter a, which was dependent on γ. The parameter s_0 on the other hand was dependent on $\sqrt{g_{tt}}$ [5] in the Einstein-Hilbert case, and dependent on $\sqrt{g_{tt}}$ and λ in the Hořava-Lifshitz case. With these two new parameters, equations 51, 53, 57 and 58 were found and used to describe the CDT data in section 3.

The χ^2_{pdf} in the number of spatial 2-simplices used per simulation shows a decreasing difference between the Einstein-Hilbert case and the Hořava-Lifshitz case for increasing time slices, and an increasing difference for increasing number of 3-simplices used. This means that, in case of the number of 2-simplices used per simulation, the Hořava-Lifshitz case only has significant better fits for data with a small number of time slices, while the number of 3-simplices used is respectively high. For data with many time slices and few 3-simplices, the difference between the Hořava-Lifshitz case and the Einstein-Hilbert case falls off. This means that while calculating these cases, the Einstein-Hilbert case gives approximately the same results as the Hořava-Lifshitz case.

In order to state anything about the χ^2_{pdf} values of the fluctuations, one has to look at the combined fits. The fits for the fluctuations alone are done with the parameter values for s_0 and a of the number of spatial 2-simplices. For the fluctuations this means that one looks at fits that are most likely not optimal. Since the dependence of χ^2_{pdf} of the fluctuations with varying parameter values is unknown, these fits could be far off.

The combined fits show an overall increase in χ^2_{pdf} with increasing number of time slices. The difference between the Einstein-Hilbert case and the Hořava-Lifshitz case shows an overall increase for $T > 21$, whereas for $T < 21$ the difference is kept relatively constant. Since the fits for the spatial number of 2-simplices used starts for $\chi^2_{pdfEH} = 98.1280$ and $\chi^2_{pdfHL} = 3.01075$ at $T = 13$, and the combined fits start at $\chi^2_{pdfEH} = 105.066$ and $\chi^2_{pdfHL} = 51.4802$, one can assume that for the fluctuations at a smaller number of time slices the Einstein-Hilbert case has a lower χ^2_{pdf} value, and thus a better fit to the data. Though, the higher the number of time slices used, the lower the difference in the χ^2_{pdf} values gets, and for $T \geq 21$ again the Hořava-Lifshitz case takes over to be the better fit to the CDT data.

At increasing numbers of 3-simplices used with a constant number of time slices $T = 25$, the exact opposite is found. For the fit of the spatial 2-simplices, the difference in χ^2_{pdf} values only grows for increasing numbers of 3-simplices. Since the combined fit has a constant difference in χ^2_{pdf} values, the Einstein-Hilbert case will have lower χ^2_{pdf} values at a high number of 3-simplices. This means that for a small number of time slices, and a high number of 3-simplices, the Einstein-Hilbert case will have a better fit to CDT data of fluctuations than the Hořava-Lifshitz case. This is opposite to what has been found for the number of spatial 2-simplices, where the Hořava-Lifshitz case has a better fit for a low amount of time slices and a high number of 3-simplices. When

[5] Out of the initial metric in expression 12.

both the number of spatial 2-simplices and the fluctuations are looked at simultaneously, the Hořava-Lifshitz case will produce better fits within the boundaries used in this thesis.

References

[1] J. Ambjørn, J Jurkiewicz and R. Loll, "Dynamically triangulating Lorentzian quantum gravity", *Nuclear Physics B* 610, (2001), 347382.

[2] J. Ambjørn, J. Jurkiewicz, and R. Loll. "Non-perturbative Lorentzian Path Integral for Gravity." *Physical Review Letters* 85 (2000) 347.

[3] J. Ambjørn, J. Jurkiewicz, and R. Loll. "Nonperturbative 3d Lorentzian Quantum Gravity." *Physical Review D* 64 (2001) 044011.

[4] R. Loll, "The Emergence of Spacetime or Quantum Gravity on Your Desktop", *arXiv:0711.0273v2*, [gr-qc], 16 Apr 2008.

[5] J. Ambjørn, J Jurkiewicz and R. Loll, "The Universe from Scratch", *arXiv:hep-th/0509010v3*, 14 Oct 2006.

[6] Joshua H. Cooperman and Jonah M. Miller, "A first look at transition amplitudes in (2 + 1)-dimensional causal dynamical triangulations", *arXiv:1305.2932v3*, [gr-qc], 15 Jan 2014.

[7] J. Ambjorn, J. Jurkiewicz, and R. Loll. "Nonperturbative 3d Lorentzian Quantum Gravity." *Physical Review D* 64 (2001) 044011.

[8] J. Ambjørn, S Jordan, J Jurkiewicz and R. Loll, "Quantum Spacetime, from a Practitioners Point of View", *arXiv:1302.2181v1*, [hep-th], 9 Feb 2013.

[9] Eric Poisson, "An advanced course in general relativity", *Department of Physics University of Guelph*, January 2002.

[10] R. K. Kommu. "A validation of causal dynamical triangulations." *Classical and Quantum Gravity* 29 (2012) 105003.

[11] Dario Benedetti and Joe Henson, "Spacetime condensation in (2+1)-dimensional CDT from a Hořava-Lifshitz minisuperspace model", *arXiv:1410.0845v1*, [gr-qc], 2 Oct 2014.

[12] C. Anderson, S. Carlip, J. Cooperman, P. Hořava, R. Kommu and P. Zulkowski, "Quantizing Hořava-Lishitz Gravity via Causal Dynamical Triangulations", *arXiv:1111.6634v1*, [hep-th], 28 Nov 2011.

[13] P. Horava. "Quantum gravity at a Lifshitz point." *Physical Review D* 79 (2009) 084008.

[14] J. Ambjørn, A. Görlich, J. Jurkiewicz, and R. Loll. "Planckian Birth of a Quantum de Sitter Universe." *Physical Review Letters* 100 (2008) 091304.

[15] J. Ambjørn, A. Görlich, J. Jurkiewicz, and R. Loll. "Nonperturbative quantum de Sitter universe." *Physical Review D* 78 (2008) 063544.